EFFECTS OF SURFACTANT ON LIFT COEFFICIENT OF ELLIPSOIDAL BUBBLES IN THE VISCOUS-FORCE DOMINANT REGIME

Chen, Junming
Hayashi, Kosuke
Legendre, Dominique
Lucas, Dirk
Tomiyama, Akio

(Citation)
Multiphase Science and Technology,35(1):55-68

(Issue Date)
2023-01-31

(Resource Type)
journal article

(Version)
Accepted Manuscript

EFFECTS OF SURFACTANT ON LIFT COEFFICIENT OF ELLIPSOIDAL BUBBLES IN THE VISCOUS-FORCE DOMINANT REGIME

Junming Chen[1], Kosuke Hayashi[1], Dominique Legendre[2], Dirk Lucas[3], Akio Tomiyama[1*]

[1]Graduate School of Engineering, Kobe University, 1-1 Rokkodai, Nada, Kobe, 657-8501, Japan

[2]Institut de Mécanique des Fluides de Toulouse (IMFT), Université de Toulouse, CNRS-INPT-UPS, 2 Allée du Professeur Camille Soula, Toulouse 31400, France

[3]Helmholtz-Zentrum Dresden-Rossendorf, Institute of Fluid Dynamics, Bautzner Landstraße 400, 01328 Dresden, Germany

*Corresponding author: tomiyama@mech.kobe-u.ac.jp

Abstract

Effects of surfactants on lift coefficients, C_L, of single ellipsoidal bubbles rising through linear shear flows were investigated. Two types of surface-active agents, i.e. Triton X-100 and 1-octanol, were used. The liquid properties except for the surface tension were identical to those in a clean system of $\log M = -5.5$, where M is the Morton number. The range of the bubble Reynolds number was $0.1 < Re < 70$. Bubble shapes were either spherical or ellipsoidal. Comparing with clean bubbles, less deformation of contaminated bubbles was confirmed. A shape correlation without taking the dimensionless shear rate into account gave good evaluations of the bubble aspect ratio, which means that the shear rate is not a dominant factor causing the change of shape deformation. However, drag coefficients were affected by the shear rate. A new correlation of drag coefficients was deduced, which agreed well with the experimental data. Both clean and contaminated C_L data showed similar tendency, i.e., after a drastic decrease in C_L, C_L slightly increases and then decreases to negative value with

increasing the bubble Reynolds number, *Re*. A difference in concentration of Trion X-100 resulted in only a slight change in C_L at high *Re* regime. Different types of surfactant resulted in noticeably different values of C_L especially at low *Re*. The C_L of small bubbles in contaminated systems could be reproduced by a correlation for solid particles, supporting that fully-contaminated spherical bubbles behave like solid spheres. For deformed bubbles, C_L can be expressed by relating the negative lift force due to shape deformation with the drag force.

Keywords: Bubble, Aspect ratio, Surfactant, Lift coefficient

1. Introduction

Two-phase flow is a ubiquitous phenomenon in both industrial processes and nature such as bubbly flows in a bubble column. Bubbles are subject to several forces causing transverse migration and non-uniform bubble distribution. Among several transverse forces, the shear-induced lift force is of great importance in modeling bubbly flows.

The lift coefficient, C_L, is used to quantify the shear-induced lift acting on a bubble (Žun, 1980). In a co-current upward bubbly flow, a positive sign of C_L makes a bubble migrate to the place where the axial component of the liquid velocity is lower while a negative sign moves a bubble in the opposite direction. Many studies have focused on a single bubble rising in liquid shear flows. Auton (1987) derived $C_L = 0.5$ for spherical bubbles at high bubble Reynolds numbers, *Re*. Žun (1980) reported that C_L of small bubbles in an air-water duct flow are positive. Legendre and Magnaudet (1997) derived C_L of spherical bubbles in linear shear flows at low *Re*, which is a function of *Re* and *Sr*, where *Sr* is the dimensionless shear rate. They also numerically found that C_L of spherical bubbles is also positive at intermediate and high *Re* and becomes almost independent of *Sr* for $Re > 10$ (Legendre and Magnaudet, 1998). As *Re* increases, C_L converges on $C_L = 0.5$, which is the theoretical value derived by Auton (1987).

Reversal migration occurs, i.e. C_L takes negative values, when the bubble shape largely departs from spherical. Tomiyama et al. (1993) predicted reversal migration for two-dimensional deformed bubbles by using an interface tracking method. Their experimental studies also showed negative values of C_L due to deformation of bubbles (Tomiyama, 1998; Tomiyama et al., 2002b). Adoua et al. (2009) pointed out that the reversal of the transverse force acting on an ellipsoidal bubble is caused by the interaction between the incident shear flow and vorticity generated at the bubble interface.

It is well-known that surface active agents, referred to as surfactant, affect bubble shape and bubble motion (Clift et al., 1978; Tomiyama et al., 2002a; Aoyama et al.,

2018). The surfactant decreases the surface tension and a non-uniform distribution of the surface tension at the bubble interface causes a tangential force to the interface, i.e. the Marangoni force, which weakens interfacial velocity and shape deformation of the bubble. The presence of surfactant also affects C_L of bubbles in linear shear flows. Fukuta et al. (2008) carried out numerical simulations using the boundary-fitted coordinate method for contaminated spherical bubbles of 0.5 mm at Re = 100 and showed dependence of C_L on the Langmuir number, La, which is the ratio of the adsorption rate to the desorption rate. Although C_L at low La agrees with the C_L value obtained by Legendre and Magnaudet (1998), C_L decreases with increasing La and changes its sign at La = 0.0448. Hayashi and Tomiyama (2018) considered surfactant effects on C_L of spherical and ellipsoidal bubbles for ranges of $2 < Re < 70$ and $Sr < 1$ using the level set method. Being similar to Fukuta's numerical results, C_L of a bubble decreases with increasing La. In association with the decrease in C_L, a sign reversal of C_L occurs at lower Re and the Eötvös number, Eo, compared with clean bubbles. They also pointed out that the Hatta number, Ha, which is the ratio of the adsorption rate to the bubble rise velocity, is an important factor to consider C_L of contaminated bubbles: C_L of high Ha bubbles can be correlated in terms of a modified Eötvös number with surface tension reduced by surfactant, whereas the Marangoni force has to be taken into account for C_L of low Ha bubbles. The influence of surfactants on the lift force in water was investigated by Hessenkemper et al. (2021). For small concentrations, an increase in the lift-force coefficient was initially observed, but it decreased again with increasing concentration and thus a decreasing aspect ratio. This effect was more pronounced for small bubbles than for larger ones. In the fully contaminated case, small C_L values were observed. Hayashi et al. (2020; 2021) proposed lift correlations applicable to bubbles in clean systems. However, no correlation, to our best knowledge, is available for contaminated systems.

For understanding the lift force acting on bubbles in contaminated systems, experimental data of C_L are still insufficient. Hence we carried out experiments on single contaminated bubbles in linear shear flows in this study. We focused on fully-contaminated bubbles, the drag coefficients of which agree with those of solid particles,

to consider a limiting case opposite to clean bubbles. The applicability of available correlations of the drag coefficient, C_D, and the aspect ratio, E, which is the ratio of the bubble minor axis to the major axis, to the present systems were examined, and a way of modelling C_L was also discussed.

2. Experimental method

Fig. 1 shows the experimental setup which consists of an acrylic tank, a stainless seamless belt with a guide, a power system for the belt rotation, a syringe and a nozzle for bubble generation, and an observation system. The width, depth and height of the tank were 200, 110, and 2100 mm, respectively, in which bubbles were rising without wall effect even with their largest size of around 4.8 mm. The stainless seamless belt of 100 mm width was tightened by two vertical parallel pulleys and was rotated by a servomotor, generating a steady linear shear flow in the 30 mm gap between the belt and the wall of the acrylic tank. The configuration was the same as in our previous study for clean bubbles (Aoyama et al., 2017), but the equipment was rebuilt for the present experiment. The velocity gradient, ω, of the linear shear flow was set at 0.0, 3.2, 4.6, 6.0 and 7.4 s^{-1}. The observation system was composed by two high-speed video cameras (Integrated Design Tools, M5; exposure time: 1/10,000s, framerate: 30-170 flames/s) mounted at z = 150 and 350 mm, respectively, to record bubble displacement for a long-time duration. The spatial resolution was in the range from 0.007 to 0.017 mm/pixel.

The sphere-volume-equivalent bubble diameter d, the bubble velocity $\boldsymbol{V}_B$, and the vertical component of the liquid velocity w_L were measured (Ogawa et al., 2007; Tomiyama, 2004; Aoyama et al., 2017). Successive bubble images were taken by using two high-speed video cameras, and d and $\boldsymbol{V}_B$ were obtained by using an image processing method (Aoyama et al., 2017). The uncertainties in d and $\boldsymbol{V}_B$ were less than 3% even for the smallest bubble. The spatiotemporal filter velocimetry (Hosokawa and Tomiyama, 2012) was employed to obtain w_L in linear shear prior to the experiments of single bubbles. We confirmed that the measured velocity gradient maintained the same level of accuracy as that in our previous study (Aoyama et al., 2017). The C_L was

calculated from the measured bubble and liquid velocities, ω and the gas and liquid densities. See Aoyama et al. (2017) for the details.

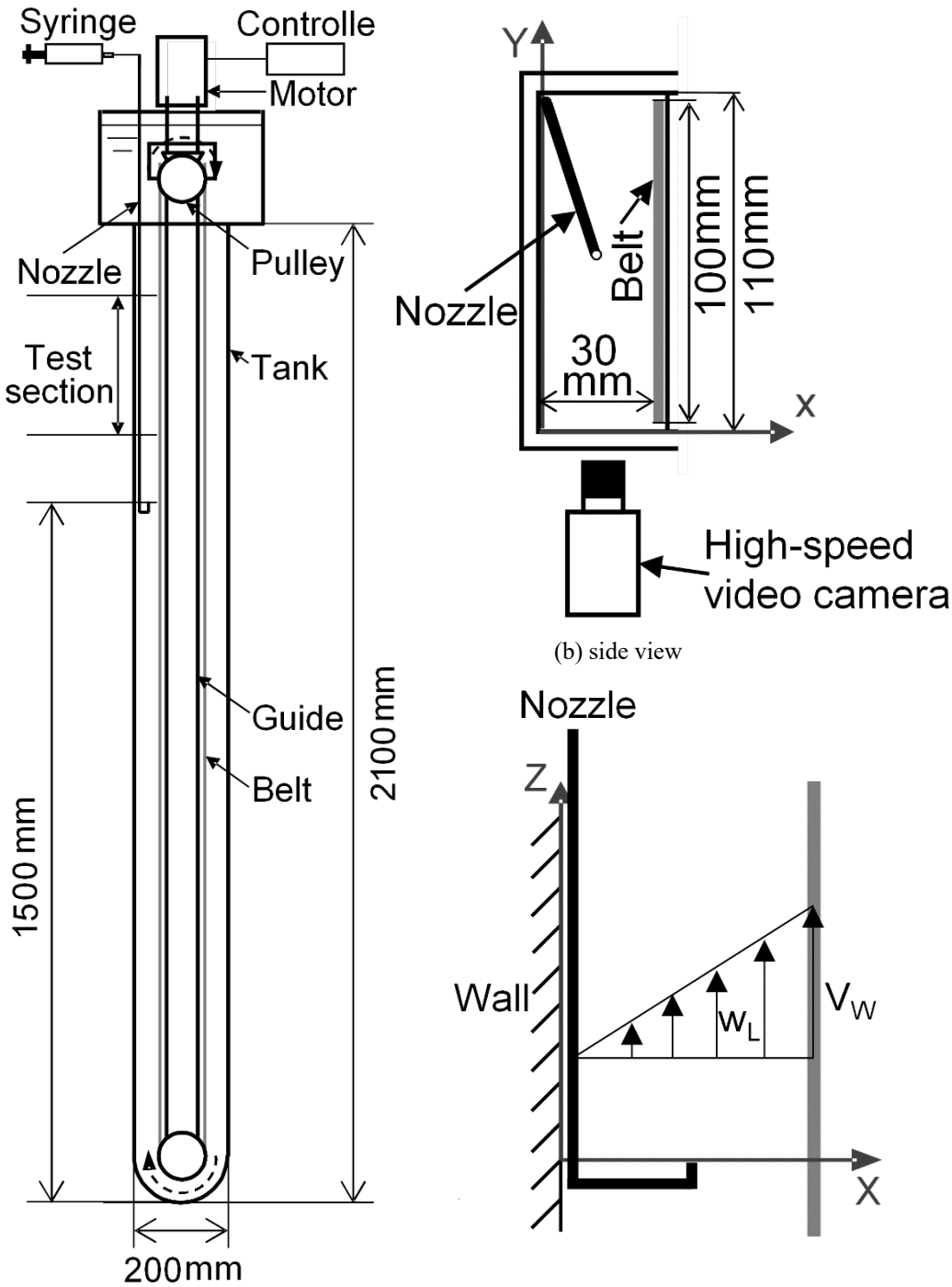

(a) Experimental setup

(b) side view

(c) Top view

Fig. 1 Experimental setup

The experiments were conducted at room temperature and atmospheric pressure. The liquid temperature was kept at 25±0.5 °C. Contaminated glycerol-water solutions and air were used as the liquid and gas phases, respectively. A clean glycerol-water solution was prepared by mixing water purified by a Millipore system (Merk, Elix 3) and pure glycerol (Kishida-Kagaku). Surfactant was then added to the solution and the solution was re-mixed. Triton X-100 (Wako Pure Chemical Industries, 168-11805) or 1-octanol (Wako Pure Chemical Industries, 156-00136) was used for surfactant. The liquid density and viscosity were measured using a densimeter (Ando keiki Co., Ltd., JIS B7525) and a viscometer (A&D, SV-10), respectively. The surface tension was measured using the pendant bubble method (Lin et al., 1990). The uncertainties in the density, viscosity and surface tension estimated at 95% confidence were 0.01, 1.3 and 2.0%, respectively.

The Morton number is defined by

$$M = \frac{\mu_L^4(\rho_L - \rho_G)g}{\rho_L^2\sigma^3} \tag{1}$$

where ρ is the density, μ the viscosity, g the acceleration of gravity, σ the surface tension, and the subscripts L and G denote the liquid and gas phases, respectively. **Table 1** shows the liquid properties, where σ_0 is the surface tension in clean systems, σ_{eq} the surface tension in adsorption-desorption equilibrium, C_T the concentration of Triton X-100, and C_O the concentration of 1-octanol. The concentration of the glycerol-water solution was 70 wt%, for which $\log M(\sigma_0)$ was −5.5. Given a further increase in surfactant concentration, no change of bubble terminal velocity suggests that the bubble is fully contaminated (Aoyama et al, 2018). We also experimented on contaminated bubbles rising through stagnant liquids for validation of fully-contaminated systems, the results of which are shown in Appendix A. The Morton number of the system contaminated with Triton X-100 was $\log M(\sigma_{eq}) \sim -5.0$, and the value of C_O was determined to realize the same Morton number $M(\sigma_{eq})$.

Table 1 Fluid properties at 25 °C (Glycerol concentration of 70 wt.% ($\log M(\sigma_0) = -5.5$))

	$\log M(\sigma_{eq})$	σ_{eq} [N/m]
Clean	–5.5	0.067
$C_T = 0.10$ mol/m^3	–5.0	0.046
$C_T = 0.20$ mol/m^3	–4.9	0.042
$C_O = 3.25$ mol/m^3	–5.0	0.047

*ρ_L = 1178 kg/m^3, ρ_G = 1.2 kg/m^3 and μ_L = 0.018 Pa·s

3. Results and discussion

3.1 *Bubble shape*

Examples of bubble shapes in the linear shear flows are shown in **Fig. 2**, where *Sr* and *Re* are defined by

$$Sr = \frac{\omega d}{|\boldsymbol{V}_R|} \tag{2}$$

$$Re = \frac{\rho_L |\boldsymbol{V}_R| d}{\mu_L} \tag{3}$$

where $\boldsymbol{V}_R$ is the bubble velocity relative to the liquid velocity. Clean bubbles measured by Aoyama et al. (2017) are also shown in the figure. The shape deformation of all contaminated bubbles is smaller than that of clean bubbles. The bubbles in the upper rows are 2.5-3.0 mm. The presence of surfactant clearly decreases C_L from 0.33 in the clean case to around zero and, in some contaminated cases C_L are negative. It should be noted that *Re* is also reduced by the presence of surfactant while the increase in *Sr* does not substantially affect C_L for these bubbles. The reduction in C_L by surfactant is also clearly observed for the larger bubbles, i.e., the decrease in C_L from the clean case is about 0.2. Negligible effects of *Sr* on C_L are again confirmed.

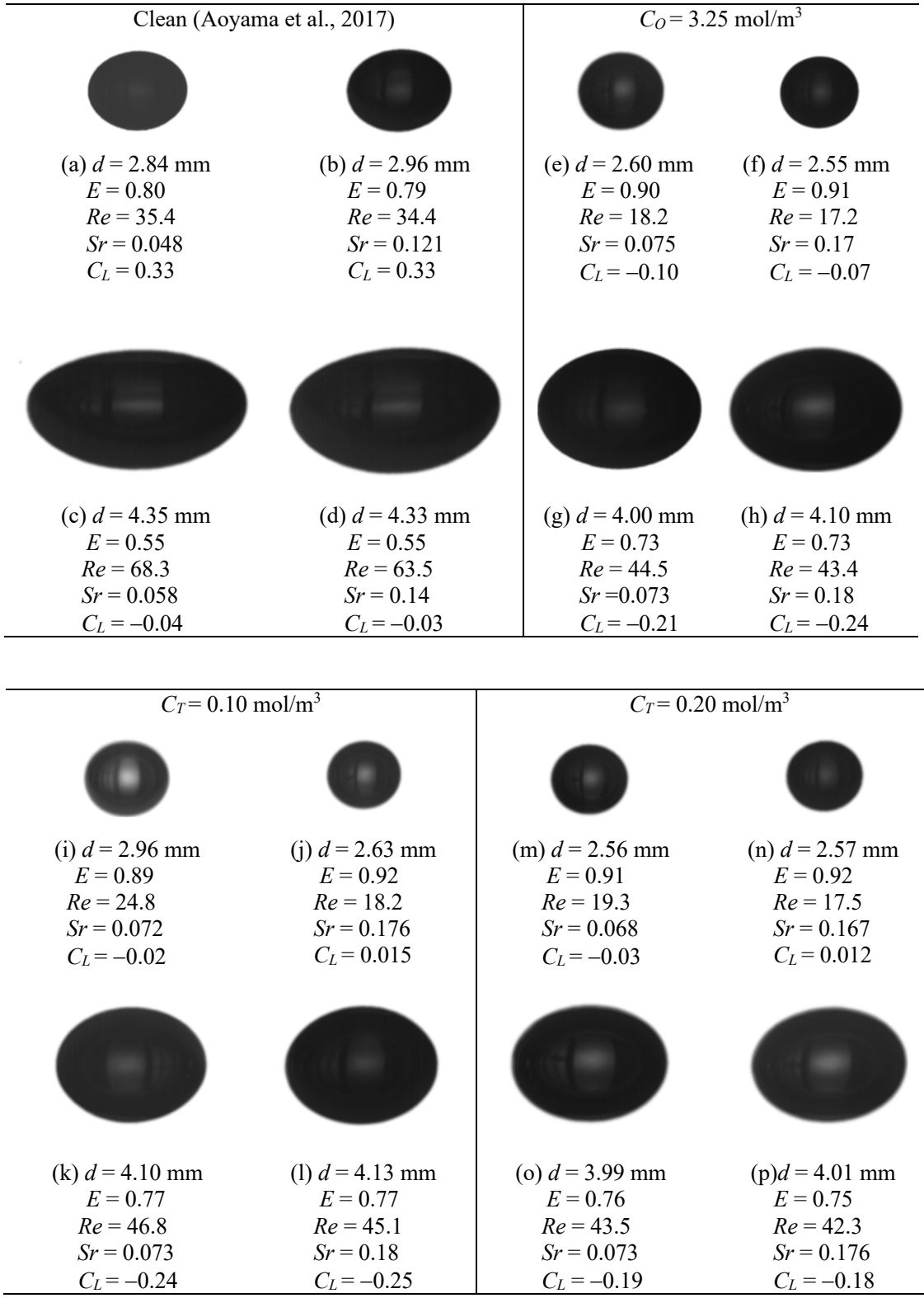

Fig. 2 Bubble shapes

3.2 *Bubble aspect ratio and relative velocity*

The aspect ratios are plotted against d in **Fig. 3**, in which the data of clean bubbles obtained by Aoyama et al. (2017) are also plotted. The E of contaminated bubbles decrease with increasing d and are larger than those of clean bubbles. The deviation from the clean bubble data increases with increasing d. The bubbles in the Triton X-100 cases show slightly weaker deformation than those in the 1-octanol case. In contrast to E, the relative velocities do not depend on the concentration and type of surfactant as shown in **Fig. 4**, i.e. the systems are fully-contaminated from the point of view of bubble velocity. The difference in E may therefore ascribe to unique absorption-desorption characteristics corresponding to a type of surfactants (Hayashi and Tomiyama, 2018). Dependence of E on Sr is not remarkable as in clean bubbles (Aoyama et al. 2017), which implies that a correlation of E for bubbles in stagnant liquids is applicable to bubbles in the linear shear flows.

Aoyama et al. (2018) proposed the following correlation of E for contaminated bubbles in stagnant liquid adopting σ_{eq} as one of its indispensable factors responsible for the shape deformation:

$$E = \frac{1}{[1+0.024Eo(\sigma_{eq})^{1.17}Re^{0.44}]^{0.57}} \tag{4}$$

Table 2 shows the mean absolute error (MAE) and root mean squared error (RMSE) of the aspect ratios calculated using Eq. (4). The correlation gives good results.

Table 2 Mean absolute error and root mean squared error in calculated aspect ratios

	MAE	RMSE
C_T = 0.10 mol/m^3	0.00471	0.00691
C_T = 0.20 mol/m^3	0.00751	0.01050
C_O = 3.25 mol/m^3	0.01340	0.01740
Average	0.00854	0.01160

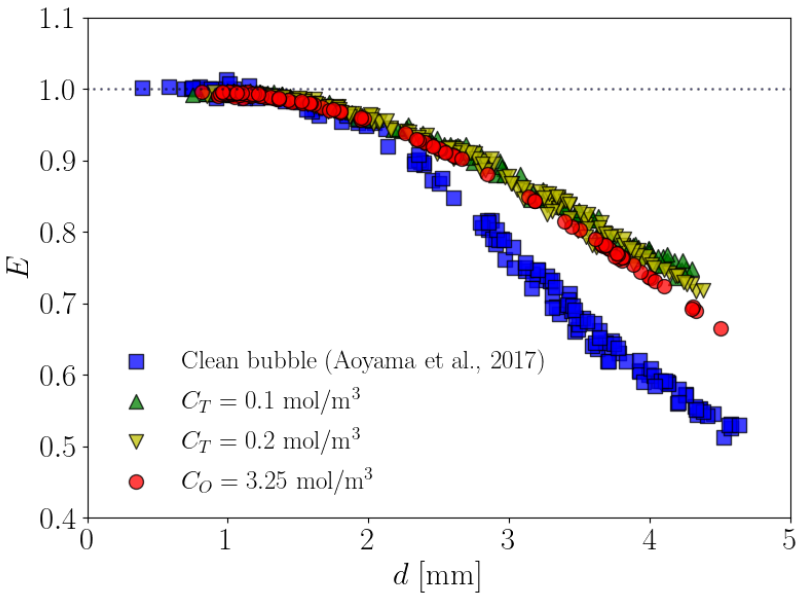

Fig. 3 Bubble aspect ratio

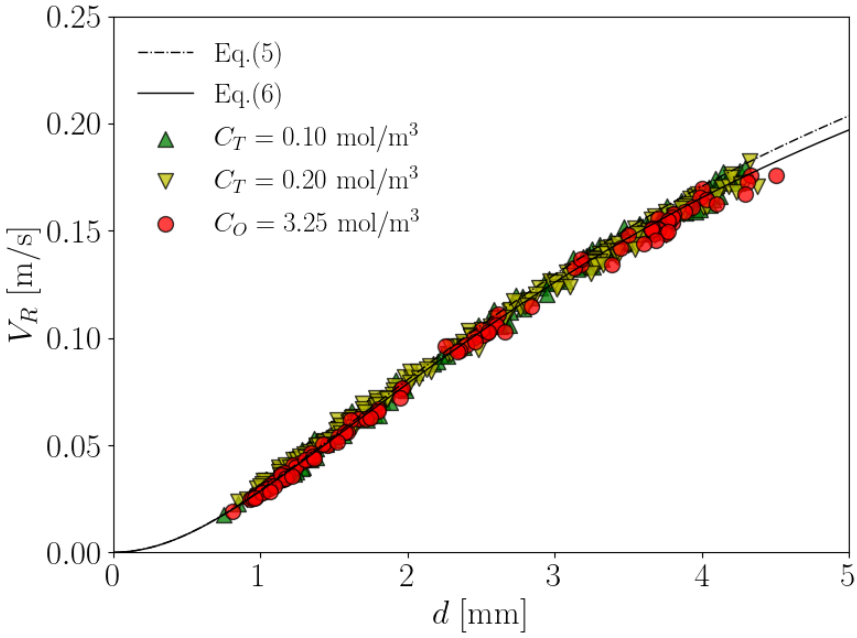

Fig. 4 Bubble relative velocity

The dotted line in **Fig. 4** represents $|\boldsymbol{V}_R|$ calculated with the following drag correlation for fully-contaminated bubbles in infinite stagnant liquids (Chen et al., 2019):

$$C_D = \frac{24}{Re}\left(1 + \frac{0.15Re^{0.687}}{E^{0.48}}\right) \tag{5}$$

where E was calculated using Eq. (4). Although the correlation gives reasonable values, the data are somewhat smaller than the curve at large d. Legendre and Magnaudet (1998) reported that C_D of spherical bubbles in shear flows increases with Sr at high Re, and developed a C_D correlation that is represented by a combination of C_D in a uniform flow and a multiplier $[1 + \alpha Sr^{\beta}]$, where α and β are constants. Aoyama et al. (2017) also recognized a slight Sr effect for clean ellipsoidal bubbles at small and intermediate Re. We obtained the following C_D correlation for contaminated bubbles with the Sr effect by adopting the multiplier with the coefficients tuned for the present data:

$$C_D = \frac{24}{Re}\left[1 + \frac{0.15Re^{0.687}}{E^{0.48}}(1 + 222Sr^{4.25})\right] \tag{6}$$

Fig. 5 shows the comparison between the $|\boldsymbol{V}_R|$ predicted by using Eq. (6) and data. By accounting for the Sr effect Eq. (6) well describes the velocity data, and MAE for Eq. (6) is 5.65 x 10^{-6} m/s, which is smaller than 1.90 x 10^{-5} m/s for Eq. (5).

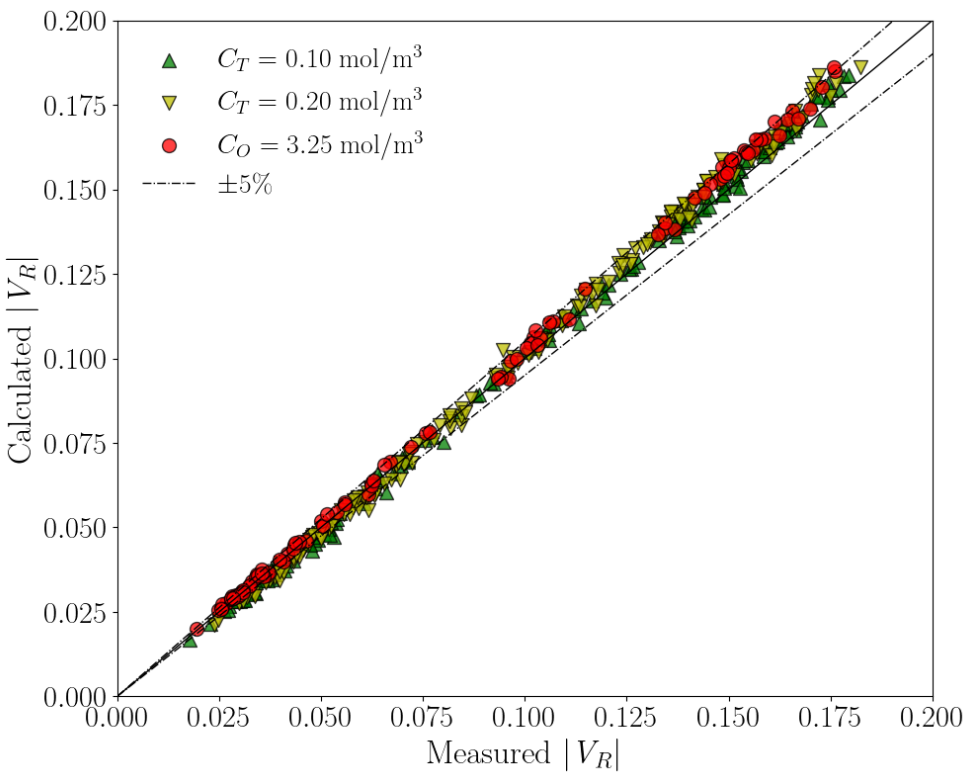

Fig. 5 Comparison between predicted and measured $|\boldsymbol{V}_R|$

3.3 Lift coefficient

Fig. 6 shows C_L of C_T = 0.10 mol/m^3 and 0.20 mol/m^3. The clean bubble data (Aoyama et al., 2017) are also plotted for comparison. Both clean and contaminated data show a similar tendency, i.e. after a steep decrease to a local minimum, further increase in *Re* causes slight increase in C_L and then decrease to the negative values. The C_L of fully-contaminated bubbles are however much lower than those of clean bubbles and the reversal of the sign of C_L due to bubble deformation occurs at smaller *Re*. The surfactant concentration shows only a small influence on C_L.

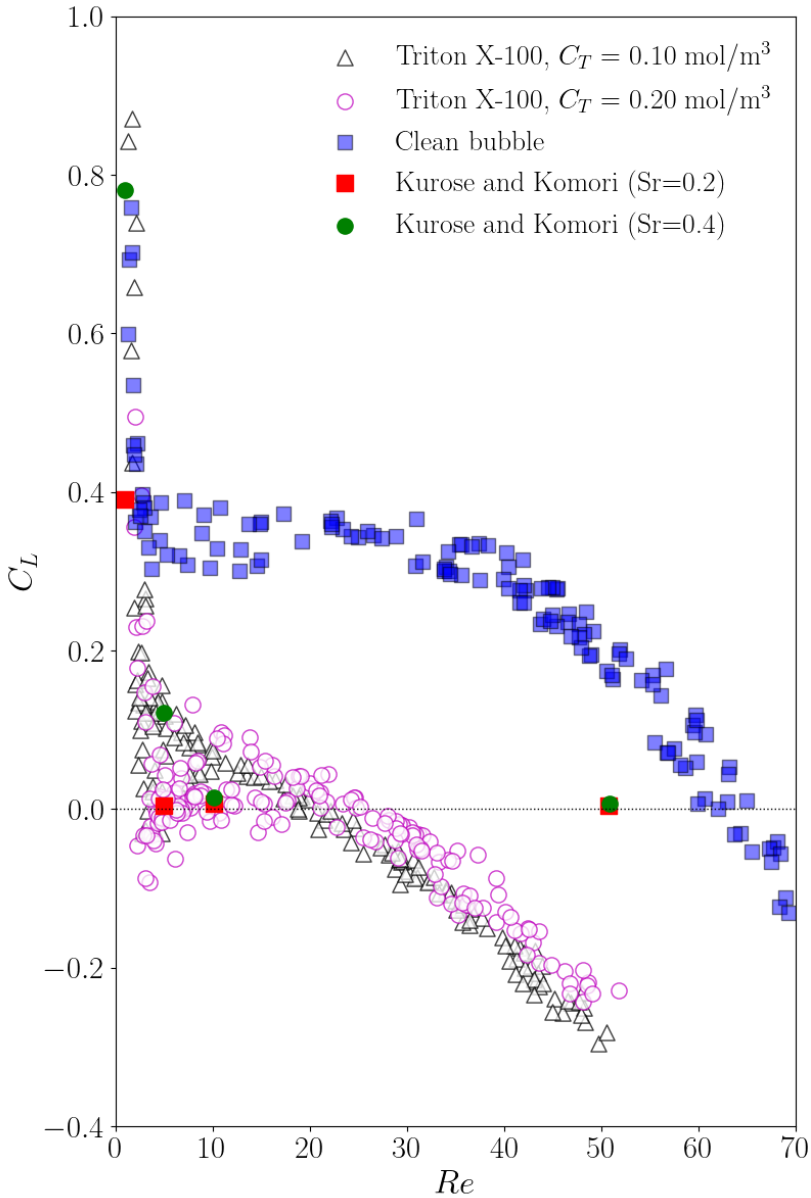

Fig. 6 Lift coefficients in clean and cases of C_T= 0.10 and 0.20 mol/m^3

It is well known that C_D of fully-contaminated spherical bubbles agree well with those of solid spheres due to the Marangoni stress. Kurose and Komori (1999) conducted numerical simulations of solid spheres in linear shear flows. Their numerical data at Sr = 0.2 and 0.4 are plotted in **Fig. 6**. The C_L of solid spheres depends on Sr for $Re \sim 5$ and becomes almost zero for $Re \geq 10$. The C_L of contaminated bubbles are close to those of solid spheres for $Re < 10$, though it is difficult to recognize clear dependence on Sr in the bubble case. As Re increases, C_L of contaminated bubbles deviate from those of solid spheres due to bubble deformation, which is similar to the relationship between clean spherical bubbles and ellipsoidal bubbles as mentioned in the introduction (Legendre and Magnaudet,1998; Aoyama et al., 2017; Hayashi et al., 2020; 2021).

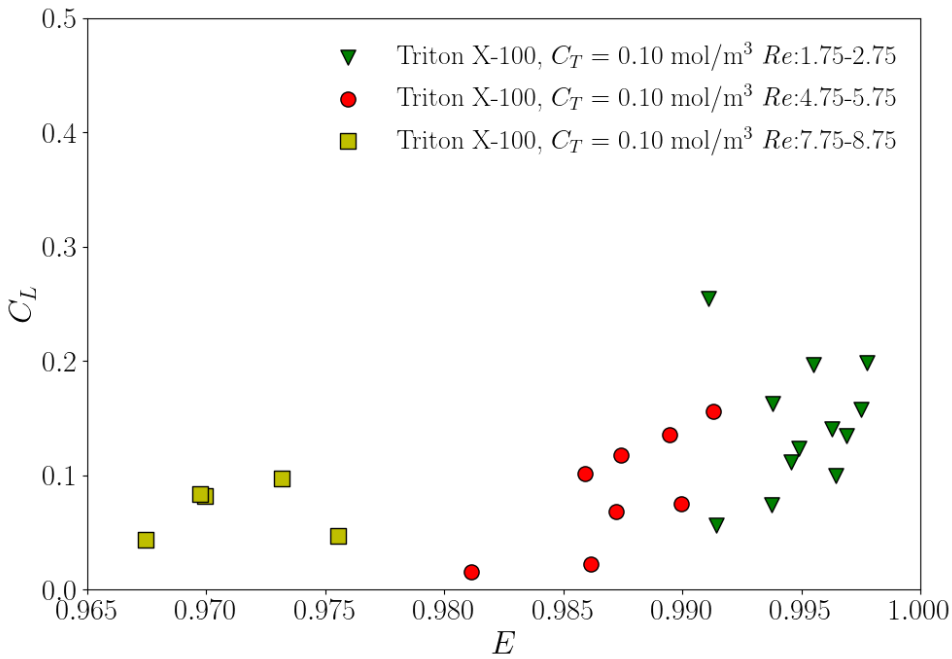

Fig. 7 C_L in Triton X-100 case at low Re range

The Triton X-100 data show some scattering in the range of Re from 2 to 20 and converges afterward. A possible explanation to this is that bubbles adopt different shapes even at the same Re due to different degree of surfactant accumulation at the interface. **Fig. 7** shows Triton X-100 data selected according to different Re ranges as indicated by the legends. It can be readily noticed that bubble shapes show a relatively

large variation even within the narrow *Re* range, which explains the reason of the scatter of C_L. The different surfactant distributions at bubble interface can be ascribed to a long time constant of surfactant adsorption/desorption, which may add uncertainties in reaching the steady state as pointed out by Zhang and Finch (2001). It is interesting that the scatter is pronounced only in the narrow *Re* range (5 ～20) and mitigates at larger *Re* where the negative lift is dominant in C_L.

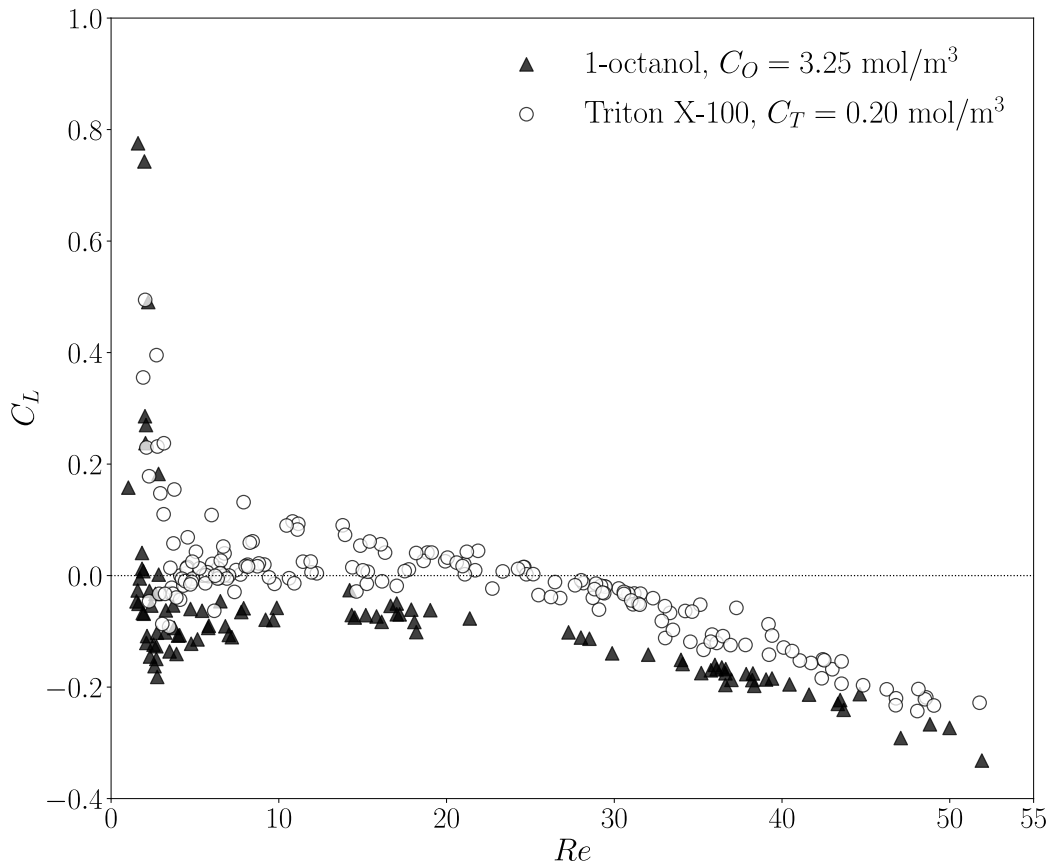

Fig. 8 Comparison between C_L of bubbles contaminated with Triton X-100 and those with 1-octanol

Fig. 8 shows C_L for two kinds of surfactants. The difference in σ_{eq} is negligibly small as shown in **Table 1**, enabling us to focus on the difference in the type of surfactants. The C_L with 1-octanol decreases to the local minimum at smaller *Re* than that with Triton X-100 and the two sets of data slightly increase and then decrease with increasing *Re*. The tendency that the deviation of these two sets of data become reduced as the increase of *Re* suggests that small bubbles are particularly subject to the ad-

desorption kinetics of surfactant, in other words the surfactant distribution at the interface, whereas shape deformation plays a dominant role in C_L as bubbles become larger. In addition, the difference between these sets of results can only be ascribed to an effect of different types of surfactants and deserves further research. The small scatter for $5 < Re < 20$ in the 1-octanol case can be described by the larger Langmuir number than in the Triton X-100 case (Hayashi and Tomiyama, 2018).

3.4 *Lift correlating*

Hayashi et al. (2020) pointed out that the drag and the negative lift of clean bubbles of $Re >> 1$ are related as

$$C_L = C_L^{S\infty} - G(\chi, Re)C_D \tag{7}$$

where $C_L^{S\infty} = 1/2$ (Auton, 1987), and $G(\chi, Re)$ is a function of χ ($= E^{-1}$) and Re. For the lift reversal in the viscous force dominant regime, they obtained the following expression of C_L, which explicitly includes the vorticity produced at the bubble interface:

$$C_L = C_L^{S\infty} - \gamma \frac{16}{Re} \phi(\chi, Re) \omega_{max}^{*\infty}(\chi) \tag{8}$$

where $\gamma = 0.078$, $\omega_{\max}^{*\infty}$ is the dimensionless maximum vorticity in the infinite Reynolds number limit given by (Magnaudet and Mougin, 2007)

$$\omega_{max}^{*\infty}(\chi) = \frac{2\chi^{5/3}(\chi^2-1)^{3/2}}{\chi^2 \sec^{-1}\chi - (\chi^2-1)^{1/2}} \tag{9}$$

and $\phi(\chi, Re)$ is the deformation-inertia factor in the drag correlation proposed by Chen et al (2019):

$$C_D = \frac{16}{Re}[1 + \phi(\chi, Re)] \tag{10}$$

where

$$\phi(\chi, Re) = 0.25\chi^{1.9}Re^{0.32} \tag{11}$$

By assuming that the negative lift of fully-contaminated bubbles has a relation similar to Eq. (7) and employing Eq. (6) for the drag, we may write

$$C_L = C_L^B - \gamma' \frac{16}{Re}\phi_c(\chi, Re)\alpha'\chi^{\beta'} \tag{12}$$

where $\phi_c(\chi, Re) = 0.15\chi^{0.48}Re^{0.68}(1 + 222Sr^{4.25})$ and $\alpha'\chi^{\beta'}$ epitomizes $\omega_{max}^{*\infty}$, whose analytical expression for rigid ellipsoids has not been obtained. The constant 16 is adopted for the factor of Re^{-1} rather than 24 since the multiplier 3/2 due to the difference in the boundary condition at the interface should be involved in $\omega_{max}^{*\infty}$ (Legendre, 2007). The C_L of a clean spherical bubble approaches 0.5 as $Re \to \infty$ and that of spherical solid particle becomes very close to zero in that limit (Kurose and Komori, 1999). In the Triton X-100 data, C_L seems to follow $C_L = 0.1$ if no deformation was assumed even at intermediate Re. On the other hand, the 1-octanol data show that C_L steeply decreases and enters to the negative lift regime at small Re. Therefore, the baseline, C_L^B, for the spherical part may be different for those cases.

The coefficients, γ', α', β' and C_L^B, were fitted to the data as shown in **Table 3**. As shown in **Fig. 9**, the C_L data in the negative lift regime can be well reproduced. For the clean bubbles, $\omega_{max}^{*\infty} \propto \chi^{8/3}$ where χ becomes large (Adoua et al. 2009). β'=6 is much larger than this limiting value for clean bubbles, implying that the contaminated interfaces with no-slip boundary condition produce larger vorticity with increasing shape deformation compared with the slip condition. The β' takes the same value in both cases, which is consistent with the fact that bubbles in both cases are fully-contaminated.

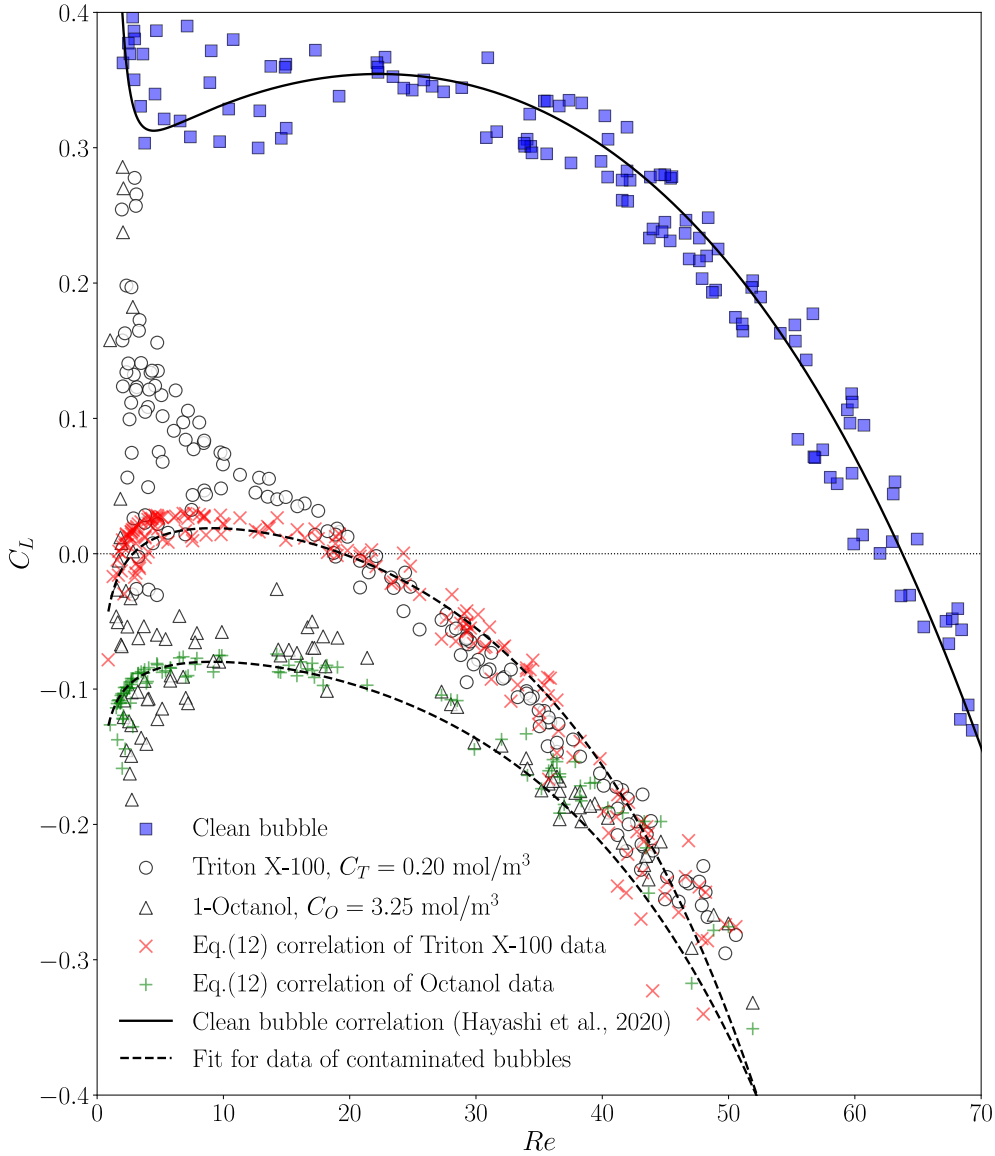

Fig. 9 Correlation of negative lift

Table 3 Coefficients in Eq. (12)

	$C_T = 0.20$ mol/m^3	$Co = 3.25$ mol/m^3
C_L^B	0.11	-0.01
$\gamma'\alpha'$	0.06	0.046
β'	6	6

4. Conclusion

Single bubbles rising in a linear shear flow of a glycerol-water solution contaminated with different types of surfactants were measured to obtain C_L data. Triton

X-100 and 1-octanol were used as surfactants. Two high-speed cameras recorded bubble lateral migration, from which bubble shapes, relative velocities and lift coefficients were obtained. The bubble Reynolds number *Re* ranged from 0.87 to 70. The dimensionless shear rate ranged from 0 to 0.25. The effect of types and concentration of surfactants on the lift coefficient were also discussed. As a result, the following conclusions were obtained:

(1) The dimensionless shear rate is not a dominant factor causing the change in shape deformation, so that an available shape correlation for bubbles in stagnant liquid can be used to estimate the bubble aspect ratio.

(2)Both clean and contaminated C_L data have similar tendency that after a drastic decrease to a local minimum, C_L value slightly increases and then gradually falls to negative lift regime.

(3) A difference in the concentration of identical surfactant results in a slight change of C_L of fully-contaminated bubbles persisting to high *Re* regime.

(4) Different types of surfactants result in different values of C_L even under the fully-contaminated condition.

(5) A negative lift component related with the drag force describes well the lift reversal for contaminated bubbles as well as for clean bubbles.

Appendix A. Rise velocities of contaminated bubbles in stagnant liquids

Figure A1 shows a comparison of relative velocities of contaminated bubbles in stagnant liquids, i.e. the terminal velocities, between measured data and Eq. (5). The measured data agree well with Eq. (5), which confirms that the present concentrations of the surfactants correspond to fully-contaminated conditions.

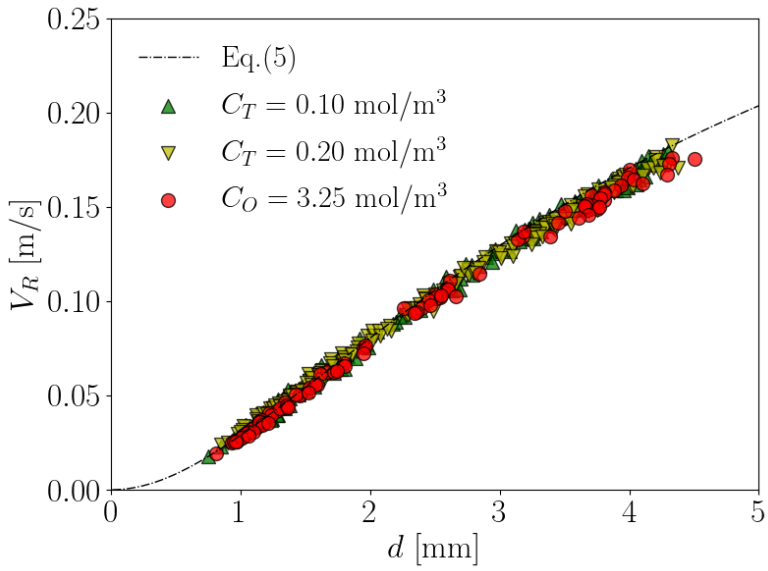

Fig. A1 Relative velocity of contaminated bubbles in stagnant liquids

References

Adoua, R., Legendre, D., and Magnaudet, D., Reversal of the Lift Force on an Oblate Bubble in a Weakly Viscous Linear Shear Flow, *J. Fluid Mech.*, vol. **628**, pp. 23-41, 2009.

Aoyama, S., Hayashi, K., Hosokawa, S., and Tomiyama, A., Lift Force Acting on Single Bubbles in Linear Shear Flows, *Int. J. Multiph. Flow*, vol. **96**, pp.113-122, 2017.

Aoyama, S., Hayashi, K., Hosokawa, S., and Tomiyama, A., Shapes of Single Bubbles in Infinite Stagnant Liquids Contaminated with Surfactant, *Exp. Therm. Fluid Sci.*, vol. **96**, pp. 460-469, 2018.

Auton, T. R., The Lift Force on a Spherical Body in a Rotational Flow, *J. Fluid Mech.*, vol. **183**, pp. 199-218, 1987.

Fukuta, M., Takagi, S., and Matsumoto, Y., Numerical Study on the Shear-induced Lift Force Acting on a Spherical Bubble in Aqueous Surfactant Solutions, *Phys. Fluids*, vol. **20**, 040704, 2008.

Hayashi, K., and Tomiyama, A., Effects of Surfactant on Lift Coefficients of Bubbles in Linear Shear Flows, *Int. J. Multiph. Flow*, vol. **99**, pp. 86-93, 2018.

Hayashi, K., Legendre, D., and Tomiyama, A., Lift Coefficients of Clean Ellipsoidal Bubbles in Linear Shear Flows, *Int. J. Multiph. Flow*, vol. **129**, 103350, 2020.

Hayashi, K., Hessenkemper, H., Lucas, D., Legendre, D., and Tomiyama, A., Scaling of Lift Reversal of Deformed Bubbles in Air-Water Systems, *Int. J. Multiph. Flow*, vol. **142**, 103653, 2021.

Hessenkemper, H., Ziegenhein, T., and Lucas, D., Contamination Effects on the Lift Force of Ellipsoidal Air Bubbles Rising in Saline Water Solutions, *Chem. Eng. J.*, vol. **386**, 121589, 2020.

Hessenkemper, H., Ziegenhein, T., Lucas, D., and Tomiyama, A., Influence of Surfactant Contaminations on the Lift Force of Ellipsoidal Bubbles in Water, *Int. J. Multiph. Flow*, vol. **145**, 103833, 2021.

Hosokawa, S., and Tomiyama, A., Spatial Filter Velocimetry based on Time-Series Particle Images, *Exp. Fluids*, vol. **52**, pp. 1361-1372, 2012.

Kurose, R., and Komori, S., Drag and Lift Forces on a Rotating Sphere in a Linear

Shear Flow, vol. **384**, pp. 183-206, 1999.

Legendre, D., and Magnaudet, J., A Note on the Lift Force on a Spherical Bubble or Drop in a Low-Reynolds-Number Shear Flow, *Phys. Fluids*, vol. **9**, pp. 3572-3574, 1997.

Legendre, D., and Magnaudet, J., The Lift Force on a Spherical Bubble in a Viscous Linear Shear Flow, *J. Fluid Mech.*, vol. **368**, pp. 81-126, 1998.

Lin, S. Y., McKeigue, K., and Maldarelli, G., Diffusion-Controlled Surfactant Adsorption Studied by Pendant Drop Digitization, *AIChE J.*, vol. **36**, pp. 1785-1795, 1990.

Ogawa, K., Myint, W., Hosokawa, S., and Tomiyama, A., Study on Lift Force Acting on Single Drops in Linear Shear Flow, *Prog. Multiph. Flow Res.*, vol. **2**, pp. 55-62, 2007 (in Japanese).

Rastello, M., Marié, J. L., and Lance, M., Drag and Lift Forces on Clean Spherical and Ellipsoidal Bubbles in a Solid-Body Rotating Flow, *J. Fluid Mech.*, vol. **682**, pp. 434-459, 2011.

Tomiyama, A., Struggle with Computational Bubble Dynamics, *Multiph. Sci. Tech.*, vol. **10**, pp. 369-405, 1998.

Tomiyama, A., Drag, Lift and Virtual Mass Forces Acting on a Single Bubble, *Proc. 3rd Int. Symposium on Two-phase Flow Modelling and Experimentation*, Pisa, 2004.

Tomiyama, A., Celata, G. P., Hosokawa, S., and Yoshida, S., Terminal Velocity of Single Bubbles in Surface Tension Force Dominant Regime, *Int. J. Multiph. Flow*, vol. **28**, pp. 1497-1519, 2002a.

Tomiyama, A., Tamai, H., Žun, I., and Hosokawa, S., Transverse Migration of Single Bubbles in Simple Shear Flows, *Chem. Eng. Sci.*, vol. **57**, pp. 1849-1858, 2002b.

Tomiyama, A., Žun, I., Sou, A., and Sakaguchi, T., Numerical Analysis of Bubble Motion with the VOF Method, *Nuclear Eng. Des.*, vol. **141**, pp. 69-82, 1993.

Zhang, Y., and Finch, J., A Note on Single Bubble Motion in Surfactant Solutions, *J. Fluid Mech.*, vol. **429**, pp. 63-66, 2001.

Žun, I., The Transverse Migration of Bubbles Influenced by Walls in Vertical Bubbly Flow, *Int. J. Multiph. Flow*, vol. **6**, pp. 583-588, 1980.